Journal of Alloys and Compounds 509 (2011) 8199–8206

Contents lists available at ScienceDirect

Journal of Alloys and Compounds

journal homepage: www.elsevier.com/locate/jallcom

Synthesis, dielectric and magnetic characteristics of poly(1-vinyl-1,2,4-triazole) (PVTri)–barium hexaferrite composite

B. Unal[a,e], Z. Durmus[b], A. Baykal[b,e,*], M.S. Toprak[c], H. Sozeri[d], A. Bozkurt[b]

[a] Department of Electrical & Electronics Engineering, Fatih University, 34500 B. Cekmece, Istanbul, Turkey
[b] Department of Chemistry, Fatih University, 34500 B. Cekmece, Istanbul, Turkey
[c] Department of Functional Materials Division, Royal Institute of Technology - KTH, SE16440 Stockholm, Sweden
[d] TUBITAK-UME, National Metrology Institute, PO Box 54, 41470 Gebze, Kocaeli, Turkey
[e] Department of BioNanoTechnology, R&D Center, Fatih University, 34500 B. Cekmece, Istanbul, Turkey

ARTICLE INFO

Article history:
Received 24 February 2011
Received in revised form 1 May 2011
Accepted 2 May 2011
Available online 23 May 2011

Keywords:
Magnetic property
Barium hexaferrite
Organic–inorganic composites
In situ polymerization
Dielectric property

ABSTRACT

The production of PVTri–$BaFe_{12}O_{19}$ composites was carried out by in situ polymerization of PVTri in the presence of synthesized $BaFe_{12}O_{19}$ particles. Crystalline phase was determined as $BaFe_{12}O_{19}$ by XRD analysis and thermal analysis revealed an inorganic content of ~45% in the composite. SEM and TEM analyses showed strongly agglomerated particles in the range of 200 nm to several micrometers in the composite. The dielectric function of the various temperatures showed frequency dependency in a reciprocal power law. The dissipation (or loss) of energy stored within the composite was found to obey the reciprocal rule of power law of the frequency dependency. The real part of electrical modulus formalism increased exponentially with frequency for various temperatures, reaching a constant value and finally saturated. The imaginary part showed a reciprocal power law against the applied frequency and shifted to higher frequency at elevated temperatures. Magnetization measurements revealed substantially lower saturation magnetization of the composite material as compared to the bulk barium ferrite powders, possibly due to pinning of some of the surface spins by the adsorption of the PVTri molecules to the surface of the $BaFe_{12}O_{19}$.

1. Introduction

Coating inorganic particles with conducting polymer to form core/shell structured materials has been demonstrated to be an effective strategy to enhance the stability of composites and widen the applications because of the strong electronic interaction between the inorganic core and polymer shell [1–3].

Barium ferrite ($BaFe_{12}O_{19}$) as M-type magnetoplumbite ferrimagnetic ceramic material, with hexagonal structure is one of the interesting candidate materials for the preparation of high-density magnetic recording media due to its fairly large magnetocrystalline anisotropy, high Curie temperature, large saturation magnetization and coercivity, and excellent chemical stability and corrosion resistivity [4–8]. The magnetic properties of barium hexaferrite originate from the Fe^{3+} ions of the barium hexaferrite structure [9]. In magnetoplumbite structure, the arrangement of the 12 Fe^{3+} ions in the unit cell is as follows: two in the tetrahedral sites (four nearest O^{2-} neighbors), nine in the dodechedral sites (six nearest O^{2-} neighbors) and one in the hexagonal site (five nearest O^{2-} neighbors) [10].

In order to obtain highly homogeneous single-domain hexagonal ferrites, several techniques have been developed, such as citrate-precursor [11], chemical co-precipitation [12], glass-crystallization [13], micro-emulsion [14], self-propagation [15] and hydrothermal [16] methods.

Studies on conducting polymers are continued to be the subject of intense investigations worldwide by many research groups [17]. Composites of conducting polymers are interesting because of their potential applications for combining properties in nanoelectronics, electromagnetics, and biomedical devices that are difficult to attain separately with individual components [18]. Among these polymer composites with inorganic nanoparticles are of particular interest because possible interactions between the inorganic nanoparticles and the polymer matrices may generate some unique physical properties upon the formation of various micro-/nanocomposites [19–24]. A number of metal or metal oxides particles have been encapsulated with conducting polymers to form composites which have found applications in electro-chromic devices, light-emitting diodes, electromagnetic interferences shielding, secondary batteries, electrostatic discharge systems, chemical and biochemical sensors, etc. [25].

* Corresponding author at: Department of Chemistry, Fatih University, 34500 B. Cekmece, Istanbul, Turkey. Tel.: +90 212 866 33 00x2061; fax: +90 212 866 34 02.
E-mail address: hbaykal@fatih.edu.tr (A. Baykal).

0925-8388/$ – see front matter © 2011 Elsevier B.V. All rights reserved.
doi:10.1016/j.jallcom.2011.05.001

As conducting polymer, poly(1-vinyl-1,2,4-triazole) is readily soluble in H_2O and DMSO, nontoxic (LD_{50} > 3000 mg/kg), biocompatible, thermally stable, and has a controllable molecular weight (10^4 to 10^6 Da) [26,27].

In this study, we report on the synthesis of barium hexaferrite/polyvinyl triazole ($BaFe_{12}O_{19}$–PVTri) composite, where $BaFe_{12}O_{19}$ is the magnetic core, and PVTri is the conductive polymeric shell. The structural, thermal, electrical, and magnetic properties of the prepared PVTri–$BaFe_{12}O_{19}$ composite were compared with that of pristine PVTri and $BaFe_{12}O_{19}$ particles. To the best of our knowledge, this is the first study on the synthesis of $BaFe_{12}O_{19}$–PVTri composite.

2. Experimental

2.1. Chemicals and instrumentations

All chemicals (1-vinyl-1,2,4-triazole (>97%, Fluka), toluene (>99%, Merck), azobisisobutyronitrile (AIBN; Merck), $Fe(CH_3COO)_2$ (from Merck)) were used as received without further purification. X-ray powder diffraction (XRD) analysis was conducted on a Rigaku Smart Lab diffractometer operated at 40 kV and 35 mA using Cu K_α radiation (λ = 1.54059 Å). Scanning electron microscopy (SEM) and transmission electron microscopy (TEM) analyses were performed, in order to investigate the microstructure of polymer and composite, using FEI XL40 Sirion FEG Digital Microscope. Samples were coated with gold at 10 mA for 2 min prior to SEM and TEM analyses. The electrical conductivity of the PVTri and PVTri–$BaFe_{12}O_{19}$ composite was studied in the range of 20–120 °C with 10 °C steps. The samples were used in the form of circular pellets of 13 mm diameter and 3 mm thickness. The pellets were sandwiched between gold electrodes and the conductivities were measured using Novocontrol dielectric impedance analyzer in the frequency range 1 Hz to 3 MHz. The dielectric data (ε' and ε'') were collected during heating as a function of frequency. VSM measurements were performed by using a Quantum Design Vibrating sample magnetometer (QD-VSM). The thermal stability was determined by thermogravimetric analysis (TGA, Perkin-Elmer Instruments model, STA 6000). The TGA thermograms were recorded for 5 mg of powder sample at a heating rate of 10 °C/min in the temperature range of 30–800 °C under nitrogen atmosphere.

2.2. Procedures

For the citrate sol–gel synthesis of $BaFe_{12}O_{19}$ (barium hexaferrite), stoichiometric amounts of $Fe(NO_3)_3$•$9H_2O$ and $Ba(NO_3)_2$ were dissolved in a minimum amount of deionized H_2O by stirring at 50 °C with Fe/Ba ratio of 12/1. Citric acid was then added to this mixture to chelate the metal ions. The molar ratios of citric acid to metal ions used were 1:1. Ammonia was added to adjust the pH value to 7. The clear solution was slowly evaporated at 80 °C under constant stirring, forming a viscous gel. By increasing the temperature up to 200 °C, the gel precursors were combusted to form brown loose powders. The precursor was precalcined at 450 °C for 4 h then, sintering at 1100 °C for 1 h was followed. The hexaferrite $BaFe_{12}O_{19}$ particles were thus obtained [28].

Azobisisobutyronitrile (AIBN; Merck) was recrystallized from THF prior to use. PVTri–$BaFe_{12}O_{19}$ composite was produced by free radical polymerization of 1-vinyl-1,2,4-triazole, in toluene using AIBN (1 mol%) as initiator, on certain amount of $BaFe_{12}O_{19}$. The reaction mixture was purged with nitrogen and the polymerization reaction was performed at 85 °C for 2 h. The resulting sample filtered and washed several times with toluene, dried in vacuum and stored in glove box.

3. Results and discussion

3.1. XRD analysis

Phase investigation of the crystallized product was performed by XRD and the diffraction pattern is presented in Fig. 1. The XRD pattern indicates that the product was M-type $BaFe_{12}O_{19}$ and the diffraction peaks were broadened owing to small crystallite size. All of the observed diffraction peaks were indexed by the hexagonal structure of $BaFe_{12}O_{19}$ (JCPDS No. 84-0757) revealing a high phase purity of hexaferrite. The mean size of the crystallites was estimated from the diffraction pattern by line profile fitting method using Eq. (1) given in [29,30]. The line profile, shown in Fig. 1 was fitted for observed 21 peaks with the following Miller indices: (1 0 4), (1 1 0), (0 0 8), (1 0 7), (1 1 4), (1 0 8), (2 0 3), (2 0 5), (2 0 6), (1 0 11), (2 0 9), (3 3 0), (2 1 7), (2 0 11), (2 0 12), (2 2 0), (1 1 14), (2 1 11), (2 0 14), (3 0 10), (2 1 12). The average crystallite, size, D and σ, was obtained as 17 ± 5 nm as a result of this line profile fitting.

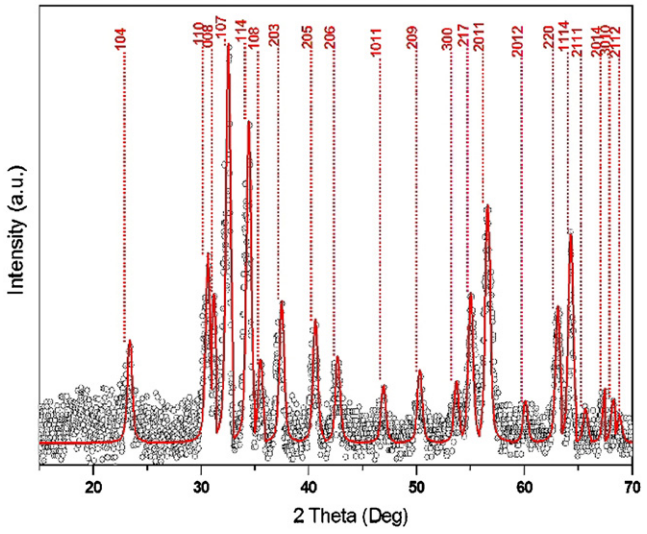

Fig. 1. XRD powder pattern and line profile fitting of PVTri–$BaFe_{12}O_{19}$ composite.

3.2. FT-IR analysis

Functional groups exhibited by uncoated $BaFe_{12}O_{19}$, PVTri, and PVTri–$BaFe_{12}O_{19}$ composite are investigated by FT-IR spectroscopy and the resultant spectra are presented in Fig. 2. As prepared powder presents characteristic peaks that were exhibited by the $BaFe_{12}O_{19}$ powder: characteristic absorption bands for $BaFe_{12}O_{19}$ at around 591 cm^{-1} and 438 cm^{-1} (corresponding to vibrations of the tetrahedral and octahedral sites for $BaFe_{12}O_{19}$) [24,31]. The triazole rings of the pristine polymer PVTri gave rise to several medium strong peaks in the 1430–1650 cm^{-1} range due to ring stretching (C–N, C=N) vibrations. The peak at 1270 cm^{-1} was assigned to the ring N–N stretching [23,32]. The broad peak centered at 3430 cm^{-1} was assigned to O–H vibration of molecular water interacting with the pristine PVTri. The spectral features of poly(1-vinylimidazole) were observed on PVTri–$BaFe_{12}O_{19}$ composite due

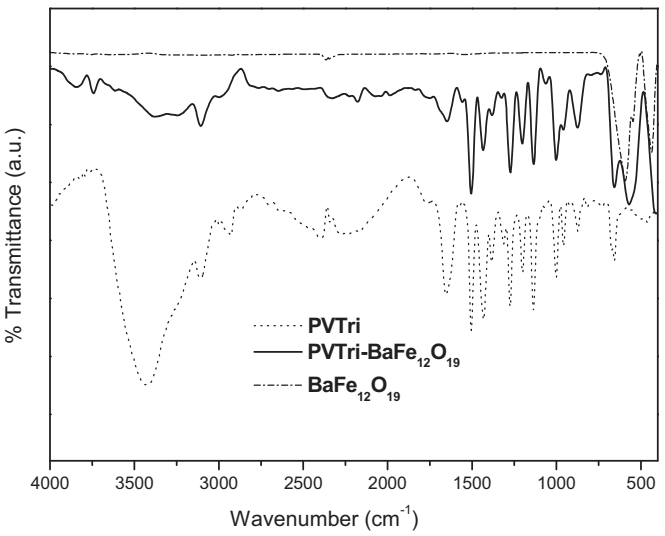

Fig. 2. FT-IR spectra of uncoated $BaFe_{12}O_{19}$, PVTri, and PVTri–$BaFe_{12}O_{19}$ composite.

to the presence of vibration bands at 1498 cm^{-1}, 1430 cm^{-1}, and 1270 cm^{-1}, respectively. These bands were absent in the spectrum of uncoated $BaFe_{12}O_{19}$ particles and confirmed the presence of PVTri on $BaFe_{12}O_{19}$.

3.3. TG analysis

Thermal stability of the material was studies by TGA and thermograms for $BaFe_{12}O_{19}$, PVTri, and PVTri–$BaFe_{12}O_{19}$ composite are presented in Fig. 3. PVTri–$BaFe_{12}O_{19}$ composite exhibited similar decomposition steps as that of PVTri, but it had a greater thermal stability. Such behavior of the composite sample may be due to the interaction between PVTri and $BaFe_{12}O_{19}$ which restricts the thermal motion of PVTri chains in the composite sample. This effect was also clearly seen in the differential thermogram (DTG) curves of such samples. DTG peak temperatures of the PVTri and PVTri–$BaFe_{12}O_{19}$ composite were almost the same. On the other hand, peak width of the DTG curve of PVTri was quite different from that of the PVTri–$BaFe_{12}O_{19}$ composite. Especially, peak half-widths could be taken into account to quantitatively compare overall degradation rates of the samples. As seen in DTG figure, peak half-width of the PVTri–$BaFe_{12}O_{19}$ composite was wider than that of PVTri. This result can be attributed to the fact that slower degradation issue for the composite than the homopolymer which clearly indicates restriction of segmental motion of polymer chains due to interactions between polymer chains and surfaces of $BaFe_{12}O_{19}$. For the homopolymer, the weight loss until 200 °C can be attributed to the removal of adsorbed water [23]. The degradation onset temperature, generally considered as the point at which degradation process begins, was found to be ~350 °C for both PVTri and PVTri–$BaFe_{12}O_{19}$ composite. For these samples, a remarkable weight loss originated from the thermal decomposition of the side groups and polymer backbone was seen above 350 °C. As expected, there was also a significant amount of residue after the completion of degradation process for the PVTri and PVTri–$BaFe_{12}O_{19}$ composite samples due to coke formation under nitrogen atmosphere for PVTri and remaining hexaferrite particles for the composite. Based on the remaining weight, composite was found to contain ~45% inorganic phase by weight.

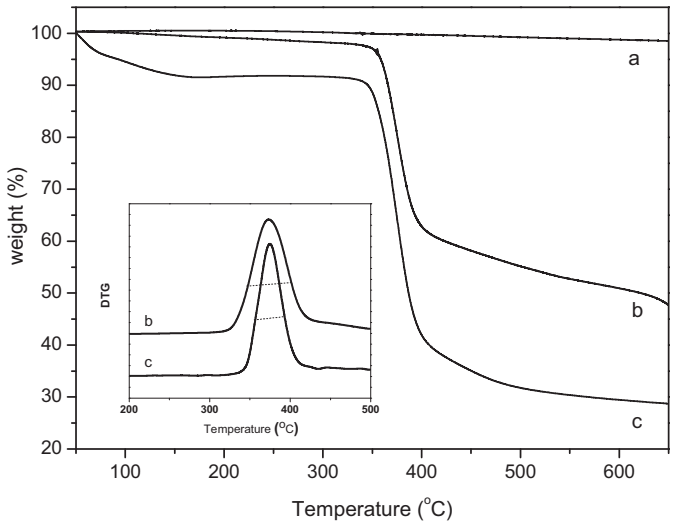

Fig. 3. TGA thermograms of (a) uncoated $BaFe_{12}O_{19}$ particles, (b) PVTri–$BaFe_{12}O_{19}$ composite, (c) PVTri and DTG (inset).

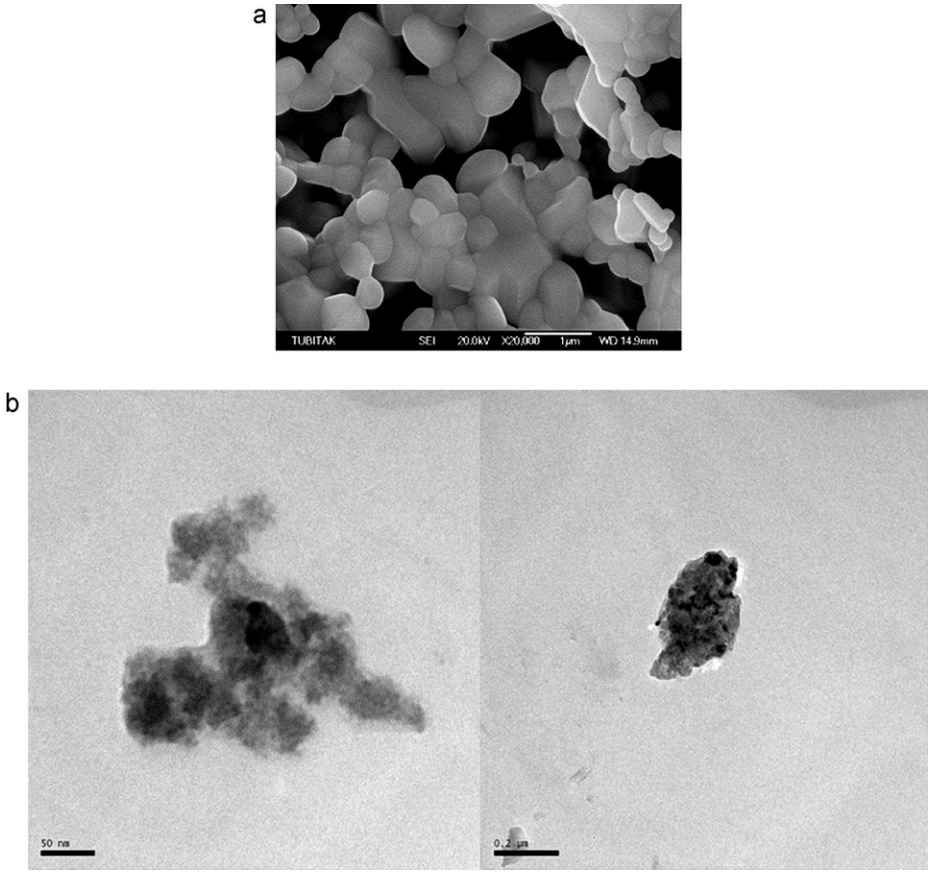

Fig. 4. (a) SEM micrograph of uncoated $BaFe_{12}O_{19}$ particles and (b) TEM micrographs of PVTri–$BaFe_{12}O_{19}$ composite.

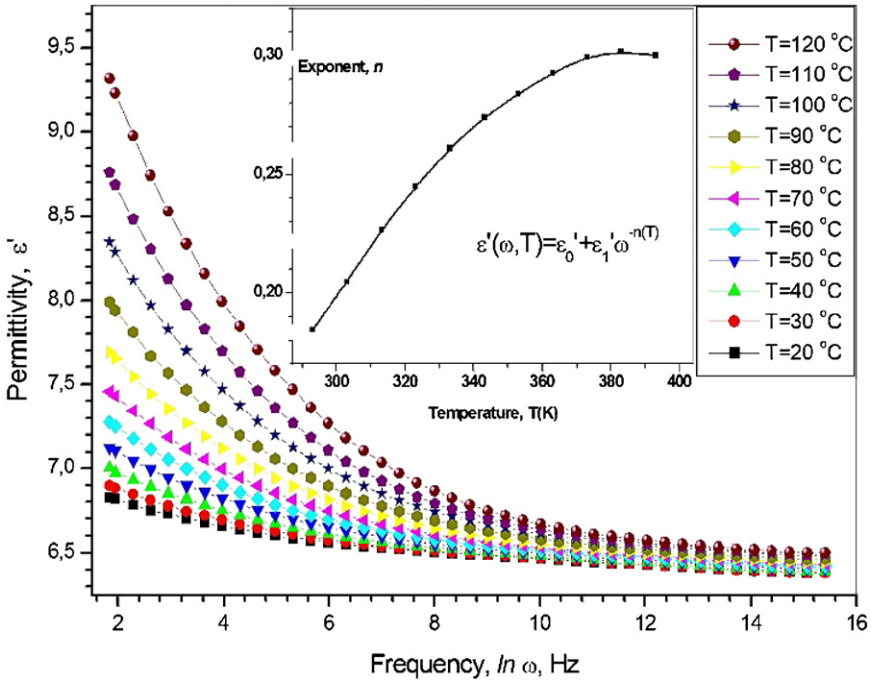

Fig. 5. The natural semilog characterisation of real part of the permittivity of PVTri–$BaFe_{12}O_{19}$ composite as a function of frequency, ω for various temperatures from RT up to 120 °C. The inset shows the variation of the exponent n with temperature.

3.4. SEM and TEM analyses

Large grains in the range from ~200 nm up to about 1 μm, having inter grain connectivity, were observed for uncoated $BaFe_{12}O_{19}$ particles (Fig. 4a). This value when compared with the crystallite size obtained from XRD line profile fitting reveals polycrystalline character of observed particles. The strong necking observed is due to the sintering process at high temperature. Microstructure of PVTri–$BaFe_{12}O_{19}$ composite was investigated by TEM and few micrographs are presented in Fig. 4b. Micrographs revealed a high degree of agglomeration of smaller particles, probably due to sintering and the nature of the polymer PVTri, forming as large as 200–300 nm pieces. Comparing SEM and TEM micrographs it was observed that the agglomeration of particles was more severe in the absence of the polymer PVTri, and the polymer helped in having a lesser extent of direct particle necking by intercalating them.

3.5. Temperature and frequency dependencies of dielectric permittivity and modulus

The natural semilog characterisation of real part (dielectric) of the permittivity of PVTri–$BaFe_{12}O_{19}$ composite as a function of frequency, ω, for various temperatures from RT up to 120 °C is illustrated in Fig. 5. The comprehensive dielectric response and near constant loss factor are, in general, associated with power law behavior, and repeatedly discovered and published as distinct properties of dielectric materials under certain conditions. Jonscher and Chanmal [33,34] discussed the fact of power law behavior in dielectric materials overwhelmingly and suggested that a more appropriate interpretation is to accept power law behavior as essential, due to the nature of many-body interactions. Therefore, real part of the permittivity as a function of frequency for various temperatures given in our study can be expressed using power law behavior as $\varepsilon'(\omega, T) = \varepsilon'_0 + \varepsilon'_1\omega^{-n(T)}$ where n is the power exponent, ε'_1 is the pre-power coefficient, and ε'_0 is the frequency-independent permittivity.

The power exponent n, pre-power coefficient ε'_1, and frequency-independent permittivity ε'_0, of the composite are plotted against temperature variation in the inset of Figs. 5 and 6, respectively. The real part of permittivity, relevant to the stored energy within the medium, reduced exponentially at all temperatures. However, the real part increased at elevated temperatures while the exponent, n, also raised with temperature. Additionally, the increase of exponent was saturated over ~90 °C. So the nature of the stored energy in the composite generated due to the applied potential across the electrodes varied with temperatures.

The characterization of the real part of permittivity, shown in Fig. 5, represented linear and parabolic variation of the components of the intersection at $\omega = 0$ and frequency multiplication, respectively as depicted in Fig. 6. In other words, ε'_0 was found to have

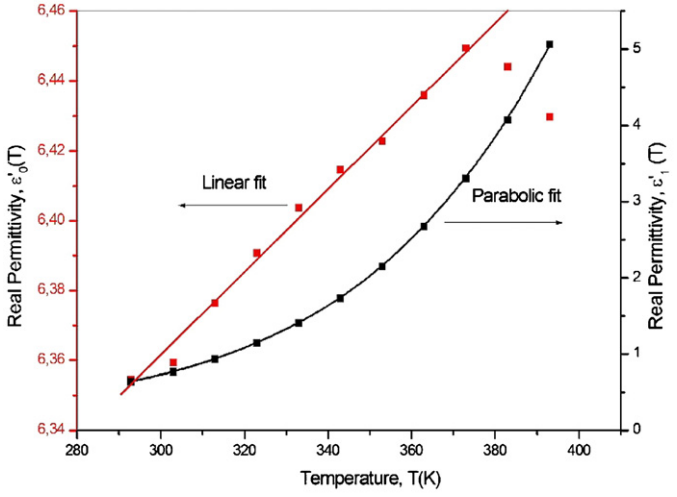

Fig. 6. The natural semilog characterisation fittings of real part of the permittivity, shown in Fig. 3, represent the linear and parabolic variation of the components of the intersection at $\omega = 0$ and frequency multiplication, respectively.

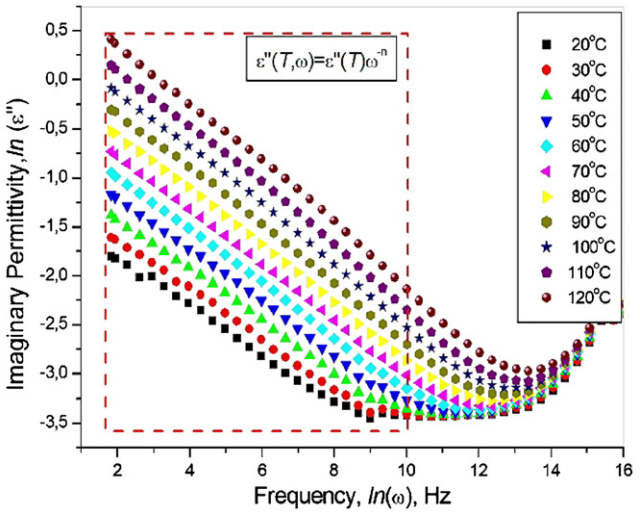

Fig. 7. The natural log–log characterisation of imaginary part of the permittivity of PVTri–$BaFe_{12}O_{19}$ composite as a function of frequency, ω for various temperatures from RT up to 120 °C (linear variation of the log–log curve represents the formula in the graph).

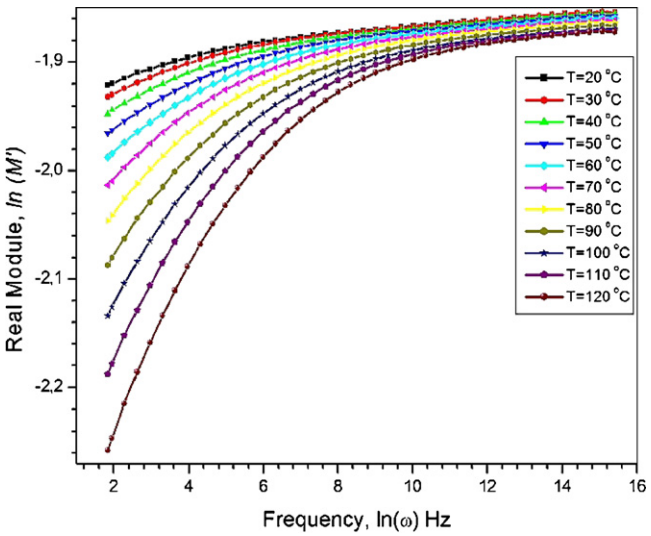

Fig. 9. The natural log–log characterisation of real part of the modulus of PVTri–$BaFe_{12}O_{19}$ composite as a function of frequency, ω for various temperatures from RT up to 120 °C.

linear dependence on temperature while pre-power coefficient of real permittivity illustrated parabolic dependence on temperature.

The imaginary part (dielectric loss) of permittivity, which is related to the dissipation (or loss) of energy within the medium, is found to be well-known attitude of the frequency dependency which can be expressed as $\varepsilon''(\omega, T) = \varepsilon''(0, T)\omega^{-n}$. Fig. 7 shows the $\varepsilon''(0, T)$ as a function of frequency for the PVTri–$BaFe_{12}O_{19}$ composite. $\varepsilon''(0, T)$ was observed to be independent of frequency in a certain range, but increased exponentially at elevated temperatures. However, the temperature dependency of power exponent n decreased exponentially at elevated temperature as shown in Fig. 8. At higher frequencies the imaginary part of permittivity became less sensitive to both frequency and temperature. These results for both real and imaginary parts of the permittivity are attributed to the ionic relaxation process although the dipolar contributions also existed at high frequency region [35,36].

Electrical modulus formalism is a quite adequate method to study the polarisation effect of composites. The electrical modulus can be calculated by the following equation [37,38]

$$M^* = (\varepsilon^*)^{-1} = M' + iM'' = \frac{\varepsilon'}{\varepsilon'^2 + \varepsilon''^2} + i\frac{\varepsilon''}{\varepsilon'^2 + \varepsilon''^2}$$

The real and imaginary parts of electric modulus of PVTri–$BaFe_{12}O_{19}$ composites are shown in Figs. 9 and 10. For all temperatures, the real part of electric modulus at lower frequencies obeyed the rule of exponential growth in the natural log-log plot. This tendency continued up to 20 kHz showing temperature dependency. Real modulus was found to be strongly temperature dependent at lower frequencies. However, at higher temperatures, the dependency level on temperature reduced remarkably, saturated and finally remained constant. Saturation of the exponentially grown real modulus in the natural log–log curve represents how the real module changes with temperature.

Figs. 9 and 10 show the real and imaginary parts of electrical modulus formalism of the PVTri-$BaFe_{12}O_{19}$ composite,

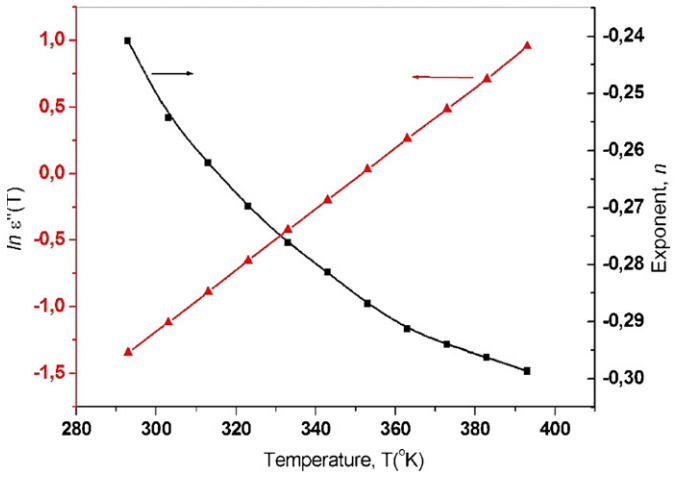

Fig. 8. The natural log–log characterisation fittings of imaginary part of the permittivity as shown in Fig. 5 represent both the linear variation of the frequency-independent imaginary permittivity components and the exponential decay of the power exponent, $n(T)$.

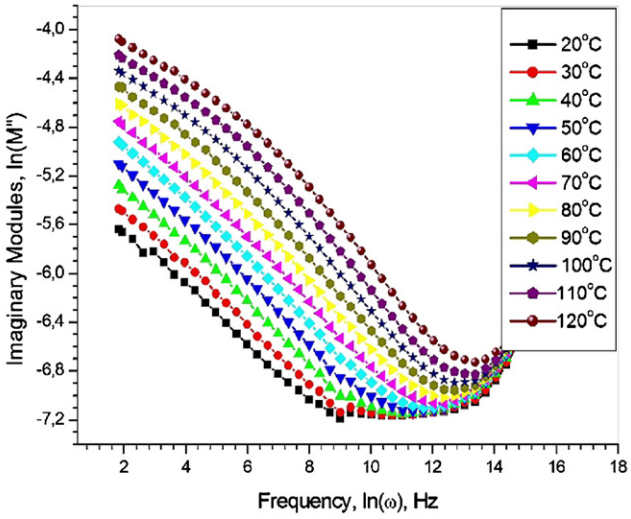

Fig. 10. The natural log–log characterisation of imaginary part of the modulus of PVTri–$BaFe_{12}O_{19}$ composite as a function of frequency, ω for various temperatures from RT up to 120 °C.

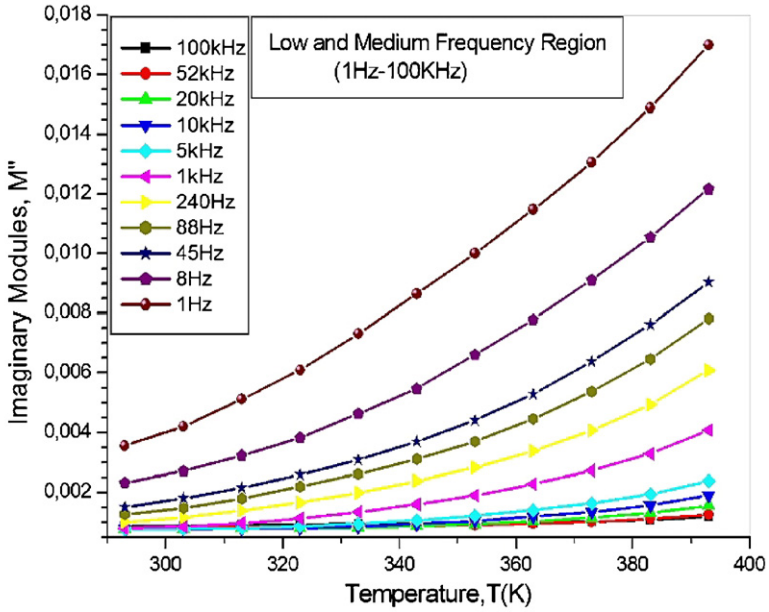

Fig. 11. The imaginary part of the modulus of PVTri–$BaFe_{12}O_{19}$ composite as a function of temperature for low and medium ranges of frequency.

respectively. Natural log–log graphs is presented in Fig. 7; the real part of modulus (M') increased exponentially with frequency for various temperatures and reached a constant value and saturated as expected, similar to that of pure L-histidine [39]. The starting points of the curves showed strongly dependency on temperature. The imaginary part (M''), roughly similar to that of imaginary part of permittivity showed a reciprocal power law against the applied frequency and shifted to higher frequency at elevated temperatures. Imaginary part varied almost linearly with frequency up to $ln\,\omega = 9$ depending upon temperature. When temperature increased, the almost linear tendency of the imaginary modulus extended, from ~3 kHz to 800 kHz. This may be attributed to the temperature-assisted-reorganization effect because of tremendous structural divergence of composite. So this type of relaxation processes can also be attributed to an interfacial polarization effects.

Imaginary part of modulus obeys the rule of the expression of $M''(\omega, T) = M''(0, T)\omega^{-n}$ at a certain limit of the frequency and also

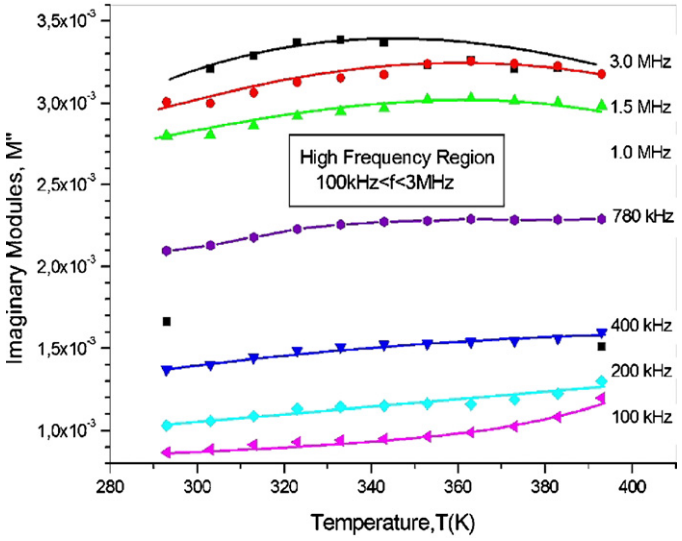

Fig. 12. The imaginary part of the modulus of PVTri–$BaFe_{12}O_{19}$ composite as a function of temperature for high frequency range over 100 kHz.

the range of variables can be extended wider while temperature changed. This can be attributed to the temperature dependency of the polarization effect at low frequency of applied electric field.

Figs. 11 and 12 show that imaginary part of modulus increased as a power law of temperature at low and medium frequency range of 1 Hz to 100 kHz while it remained almost constant for all temperatures in the frequency range over 100 kHz up to 3 MHz.

According to the electrical modulus formalism, the temperature and frequency dependencies of dielectric properties of the PVTri–$BaFe_{12}O_{19}$ composite can be explained as follows [40,41]: when the temperature is lowered, the expansion of PVTri–$BaFe_{12}O_{19}$ composite will separate the filling components of the composite. The interfaces between $BaFe_{12}O_{19}$ and PVTri matrix will enhance, and the dielectric constant will rise. When the temperature is higher than a certain value, the PVTri crystalline phase begins to change, transforming from a semi-crystalline phase to the polymer-like phase. The interfaces between the $BaFe_{12}O_{19}$ and the PVTri matrix will decrease causing the decrease of the dielectric constant and increased polarization. In this case, the dielectric constant increases again. At higher frequency, the values of the electric modulus of both PVTri and the composite become less temperature-dependent. Overall, there are a few different number of mechanisms which influence the shape of the permittivity through a certain frequency range: Relaxation effects are known to be associated with permanent and induced molecular dipoles. At lower frequency the applied electric field varies slowly enough to allow dipoles to reach equilibrium before the field has measurably changed. For higher frequencies at which dipole orientations cannot track the applied field due to the viscosity of the medium, the absorption of the field energy results in energy dissipation. The mechanism of dipoles relaxing is termed as dielectric relaxation. Resonance effects originate from the rotations or vibrations of atoms, ions, or electrons. These processes are examined in the neighborhood of their characteristic absorption frequencies [42,43].

3.6. Magnetic characteristics

Magnetic properties of the PVTri–$BaFe_{12}O_{19}$ composite was investigated by measuring $M(H)$ hysteresis, isothermal (IRM) and

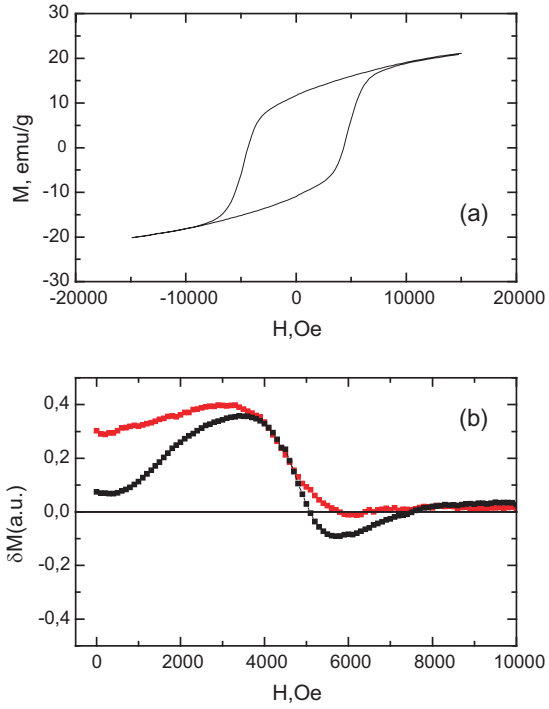

Fig. 13. Magnetic evaluation of PVTri–$BaFe_{12}O_{19}$ composite (a) *M–H* curve, (b) Magnetic interactions deduced from the Stoner-Wohlfarth model.

demagnetization remanence (DMD) curves at room temperature up to an external field of 15 kOe. M(H) hysteresis curve, Fig. 13a, evidently showed that sample was not saturated at maximum applied field. Thus, saturation magnetization of the composite was determined, by extrapolating the *M* vs. $1/H$ plots for $1/H \rightarrow 0$, as 24.3 emu/g which is considerably lower compared to bulk $BaFe_{12}O_{19}$ (64.3 emu/g) [44,45]. Considering the fact that composite contained only ~45% inorganic phase, when saturation magnetization was normalized for the content of $BaFe_{12}O_{19}$ a value of 54 emu/g was obtained. This reduction in saturation magnetization can be explained by the adsorption of the non-magnetic molecules PVTri on the surface of $BaFe_{12}O_{19}$ particles, which results in the formation of dead magnetic layer and causes spins of the metallic ions to be pinned. Thus, these spins cannot make contribution to the overall magnetization. In some ferrimagnetic systems like Mn [46] and Ni ferrites [47], this reduction was attributed to the finite size effects namely the canting of the surface spins due to the reduced exchange coupling with the core spins. However, there is no observation of spin canting in ferromagnetic oxides. The Mr/Ms ratio depends on grain size and its distribution in such a way that small grain size and homogeneous distribution produces higher Mr/Ms ratio. This ratio is close to the 0.5 for non-interacting particles [48] and it is 0.47 in our composite. Magnetic interactions between the hard ($BaFe_{12}O_{19}$) and impurity phases, like hematite (α-Fe_2O_3) or barium monoferrite ($BaFe_2O_4$) that could be present even if they are not detected in XRD patterns, can be calculated using the Stoner–Wohlfarth model. It should be noted that positive (negative) values of $\delta M(H)$ in Fig. 13b correspond to the magnetizing-like (demagnetizing-like) interactions, which try to stabilize (destabilize) the remanence. Fig. 13b indicates that there is a magnetizing-like interaction up to 5 kOe that stabilizes the remanence and weak demagnetizing type interaction appears between 5 and 7 kOe in the bulk sample. In higher fields, these phases can be considered as non-interacting. For the composite material, we can state that magnetizing-like interaction becomes stronger compared to bulk sample up to 8 kOe and can be considered as non-interacting above it. Coating $BaFe_{12}O_{19}$ particles with PVTri decreases the Ms of the bulk material; on the other hand, it enhances the magnetizing-like interactions in a wide field range up to 10 kOe.

4. Conclusions

We presented the synthesis of PVTri–$BaFe_{12}O_{19}$ composite fabrication for the first time via one-pot in situ polymerization of PVTri in the presence of freshly synthesized $BaFe_{12}O_{19}$. Crystalline product was determined as $BaFe_{12}O_{19}$ by XRD analysis and thermal analysis revealed an inorganic content of ~45% in the composite. Aggregation and agglomeration of particles into micrometer large pieces was observed by SEM and TEM analyses. The dielectric permittivity of PVTri–$BaFe_{12}O_{19}$ composite was found to obey a power law formula of reciprocal function of frequency for both dielectric permittivity (ε') and dielectric loss (ε''). Additionally, the power exponent was also found to be temperature dependent. The real part of electrical modulus formalism increased exponentially with frequency for various temperatures, reaching a constant value and saturated. Saturation magnetization (Ms) of the composite was considerably lower compared to bulk. Adsorption of the PVTri molecules to the surface of $BaFe_{12}O_{19}$ particles, that is also confirmed by FT-IR analysis, is suggested for the observed reduction in Ms. Investigation of magnetic interactions between hard and impurity phases in bulk and composite revealed that strength of magnetizing-like interactions is higher in wide field range in the composite material.

Acknowledgements

The authors are thankful to the Fatih University, Research Project Foundation (Contract no: P50020902-2), Scientific and Technological Research Council of Turkey (TÜBİTAK) (Project no:110T487) for financial support of this study. MST acknowledges the fellowship from Knut and Alice Wallenbergs Foundation (No: UAW2004.0224). H.Sozeri thanks to Cem İpek and Dr. Özgür Duygulu for SEM and TEM images.

References

[1] K. Singh, A. Ohlan, A.K. Bakhshia, S.K. Dhawan, Mater. Chem. Phys. 119 (2010) 201.
[2] S. Tian, J. Liu, T. Zhu, W. Knoll, Chem. Mater. 16 (2004) 4103.
[3] Y. Li, G. Chena, Q. Li, G. Qiua, X. Liu, J. Alloys Compd. 509 (2011) 4104.
[4] R. Sharma, R.C. Agarwala, V. Agarwala, Mater. Lett. 62 (2008) 2233.
[5] F. Mou, J. Guan, Z. Sun, X. Fan, G. Tong, J. Solid State Chem. 183 (2010) 736.
[6] H.M. Leea, Y.J. Kima, J.H. Ahn, J. Alloys Compd. 504S (2010) S332–S335.
[7] V.N. Dhage, M.L. Mane, M.K. Babrekar, C.M. Kale, K.M. Jadhav, J. Alloys Compd. 509 (2011) 4394–4398.
[8] G. Murtaza Rai, M.A. Iqbal, K.T. Kubra, J. Alloys Compd. 495 (2010) 229–233.
[9] H.Z. Wang, Q. He, G.H. Wen, F. Wang, Z.H. Ding, B. Yao, J. Alloys Compd. 504 (2010) 70–75.
[10] Q. Mohsen, J. Alloys Compd. 500 (2010) 125–128.
[11] H.F. Yu, P.C. Liu, J. Alloys Compd. 416 (2006) 222–227.
[12] P. Shepherd, K.K. Mallick, R.J. Green, J. Magn. Magn. Mater. 311 (2007) 683–692.
[13] E.A. Gravchikova, D.D. Zaitsev, P.E. Kazin, J. Inorg. Mater. 42 (2006) 914–917.
[14] P. Xu, X.J. Han, M.J. Wang, J. Phys. Chem. C 111 (2007) 5866–5870.
[15] I.P. Parkin, Q.A. Pankhurst, G. Elwin, Adv. Mater. 8 (1997) 643–645.
[16] M. Drofenik, I. Ban, D. Makovec, A. Žnidaršič, Z. Jagličić, D. Hanžel, D. Lisjak, Mater. Chem. Phys. 127 (2011) 415–419.
[17] S. Palaniappa, A. John, Prog. Polym. Sci. 33 (2008) 732.
[18] A. De, P. Sen, A.P. Addar, A. Das, Synth. Met. 159 (2009) 1002.
[19] Z. Durmus, H. Erdemi, A. Aslan, M.S. Toprak, H. Sozeri, A. Baykal, Polyhedron 30 (2011) 419.
[20] C. Basavaraja, E.A. Jo, D.S. Huh, Mater. Lett. 64 (2010) 762.
[21] Z. Durmus, B. Unal, M.S. Toprak, A. Aslan, A. Baykal, Physica B 406 (2011) 2298.
[22] Z. Durmus, H. Kavas, A. Baykal, H. Sozeri, L. Alpsoy, S.U. Celik, M.S. Toprak, J. Alloys Compd. 509 (2011) 2555.
[23] H. Kavas, Z. Durmus, A. Baykal, A. Aslan, A. Bozkurt, M.S. Toprak, J. Non-Cryst. Sol. 356 (2010) 484.
[24] B. Birsöz, A. Baykal, H. Sözeri, M.S. Toprak, J. Alloys Compd. 493 (2010) 481.
[25] K.R. Reddy, K.P. Lee, A.J. Kopalan, Colloid Surf. A 320 (2008) 49.
[26] G.F. Myachina, S.A. Korzhova, T.G. Ermakova, B.G. Sukhov, B.A. Trofimov, Doklady Chem. 420 (2008) 123.

[27] T.G. Ermakova, N.P. Kuznetsova, L.I. Volkova, G.F. Myachina, Russian J. Appl. Chem. 82 (2009) 488.
[28] Z. Durmus, B. Unal, M.S. Toprak, H. Sozeri, A. Baykal, Polyhedron 30 (2011) 1349.
[29] T. Wejrzanowski, R. Pielaszek, A. Opalińska, H. Matysiak, W. Lojkowski, K.J. Kurzydlowski, Appl. Surf. Sci. 253 (2006) 204.
[30] R. Pielaszek, Analytical expression for diffraction line profile for polydispersive powders, in: Proceedings of the XIX Conference, Krakow, Poland, Applied Crystallography (2003) 43.
[31] T. Gonzaılez-Carreno, M.P. Morales, C.J. Serna, Mater. Lett. 43 (2000) 97.
[32] S.Ü. Çelik, A. Aslan, A. Bozkurt, Solid State Ionics 179 (2008) 683.
[33] A.K. Jonscher, Dielectric Relaxation in Solids, Chelasea Dielectric Press, London, 1983.
[34] C.V. Chanmal, J.P. Jog, eXPRESS, Polym. Lett. 2 (2008) 294.
[35] D.J. Griffiths, Introduction to Electrodynamics, 3rd ed., Prentice Hall, New York, 1998.
[36] J.D. Jackson, Sect. 7.5.B and 7.5C, in: Classical Electrodynamics, 3rd ed., Wiley, New York, 1999.
[37] G.M. Tsangaris, O.C. Psarras, N. Kouloumbi, J. Mater. Sci. 33 (1998) 2027.
[38] S. Abdul-lawad, A. Alnajjar, M.H. Abdallah, Appl. Phys. A: Mater. Sci. Process. 64 (1997) 199.
[39] B. Ünal, Z. Durmuş, A. Baykal, H. Sözeri, M.S. Toprak, L. Alpsoy, J. Alloys Compd. 505 (2010) 172.
[40] S. Yu, P. Hing, X. Hu, J. Appl. Phys. 88 (2000) 398.
[41] V. Bobnar, A. Levstik, C. Huang, Q.M. Zhang, J. Non-Crys. Sol. 353 (2007) 205.
[42] K. Dillip, R. Pradhan, N.P. Choudhary, B.K. Samantaray, Int. J. Electrochem. Sci. 3 (2008) 597.
[43] B. Unal, Z. Durmus, H. Kavas, A. Baykal, M.S. Toprak, Mater. Chem. Phys. 123 (2010) 184.
[44] H. Sözeri, J. Magn. Magn. Mater. 321 (2009) 2717.
[45] H. Sözeri, J. Alloys Compd. 486 (2009) 809.
[46] Z.X. Tang, C.M. Sorensen, K.J. Klabunde, G.C. Hadjipanayis, J. Appl. Phys. 69 (1991) 5279.
[47] R.H. Kodama, A.E. Berkowitz, E.J. McNiff, S. Foner, Phys. Rev. Lett. 77 (1996) 394.
[48] J.F. Wang, C.B. Ponton, R. Grössinger, I.R. Harris, J. Alloys Compd. 369 (2004) 170.